

Spin-Spin Correlations in the Kitaev Model at Finite Temperatures: Approximate and Exact Results via Green's Function Equation of Motion

Hibiki Takegami* and Takao Morinari†

Course of Studies on Materials Science, Graduate School of Human and Environmental Studies, Kyoto University, Kyoto 606-8501, Japan

(Dated: July 18, 2024)

The Kitaev model, defined on a honeycomb lattice, features an exactly solvable ground state with fractionalized Majorana fermion excitations, which can potentially form non-Abelian anyons crucial for fault-tolerant topological quantum computing. Although Majorana fermions are essential for obtaining the exact ground state, their physical interpretation in terms of spin operators remains unclear. In this study, we employ a Green's function approach that maintains SU(2) symmetry to address this issue and explore the model's finite temperature properties. Our results demonstrate that the computed temperature dependence of the correlation functions closely approximates the exact values at zero temperature, confirming the accuracy of our method. We also present several exact results concerning the spin Green's function and spin-spin correlation functions that are specific to the Kitaev model.

Quantum spin liquids have emerged as a central topic in condensed matter physics, capturing significant attention due to their complex and intriguing properties¹. Among the various theoretical models, the Kitaev model is particularly notable for its exactly solvable ground state, which features fractionalized Majorana fermions². This model is not only analytically tractable but also holds potential for real-world applications in materials with significant spin-orbit coupling^{3,4}. Majorana fermions play a crucial role in the development of topological quantum computers, offering a platform for fault-tolerant quantum computation^{5,6}.

While investigating the Kitaev model in terms of Majorana fermions provides significant mathematical elegance, a deeper understanding of the physical nature of Majorana fermions may be achieved through the study of spin operators. However, the Kitaev model presents substantial challenges due to its highly frustrated and strongly correlated nature.

In this paper, we employ the spin Green's function approach for the spin operators while preserving SU(2) symmetry and solve its equation of motion. This method, which maintains SU(2) symmetry⁷, is particularly suitable because the system does not exhibit magnetic long-range order even at zero temperature. Another critical observation is that the spin-spin correlation function in the ground state is finite only between nearest neighbor sites⁸, suggesting that the spin-spin correlation length remains short-ranged even at finite temperatures. Since the equation of motion for the Green's function⁹ relies on finite-range correlation functions, it is well-suited for exploring the finite temperature properties of the Kitaev model. Additionally, this approach aligns with the high-temperature expansion⁷, enhancing the accuracy of results at higher temperatures. Physically, our spin Green's function describes the propagation of a pair of \mathbb{Z}_2 fluxes. Our results demonstrate that the computed temperature dependence of the correlation functions yields a value at zero temperature that is quite close to the exact value. Furthermore, we present several exact results regarding

spin-spin correlation functions at finite temperatures.

The Hamiltonian of the isotropic Kitaev model on the honeycomb lattice is given by²:

$$\mathcal{H} = -K \sum_{\gamma=x,y,z} \sum_{\langle i,j \rangle_{\gamma}} S_i^{\gamma} S_j^{\gamma}, \quad (1)$$

where S_i^{γ} is the γ -component of the spin-1/2 operator at site i , and we consider the ferromagnetic Kitaev coupling $K > 0$. The summation of $\langle i,j \rangle_{\gamma}$ represents the sum over the nearest neighbor sites connected by a γ bond, as shown in Fig. 1. In the honeycomb lattice, each unit cell comprises two sites corresponding to the A and B sublattices, as illustrated in Fig. 1. Additionally, Fig. 1 shows a plaquette p consisting of six sites. For this plaquette, we define the following plaquette operator²:

$$W_p = \sigma_1^x \sigma_2^y \sigma_3^z \sigma_4^x \sigma_5^y \sigma_6^z, \quad (2)$$

where σ_i^{γ} represents the γ -component of the Pauli matrix at site i . σ_i^{γ} can be expressed as $\sigma_i^{\gamma} = ib_i^{\gamma} c_i$ in terms of two types of Majorana fermions², where this equality holds by restricting the extended Hilbert space of Majorana fermions to the physical Hilbert space of the original spin operators. The product of two Majorana fermions, b_i^{γ} and b_j^{γ} , residing at nearest neighbor sites forms a \mathbb{Z}_2 gauge field. In this formulation, W_p represents the \mathbb{Z}_2 gauge flux. Meanwhile, the Majorana fermions c_i are itinerant under these \mathbb{Z}_2 gauge fields.

An intriguing aspect of the Kitaev model is that it has been rigorously demonstrated that its ground state is a spin liquid state without long-range magnetic order. Because of the absence of the magnetic long-range order, we may apply SU(2) invariant formalism of the Green's function method⁷. We define the Matsubara Green's function:

$$G_{n\alpha_1, m\alpha_2}^{\gamma}(\tau) = -\langle T_{\tau} S_{n\alpha_1}^{\gamma}(\tau) S_{m\alpha_2}^{\gamma}(0) \rangle \equiv \langle S_{n\alpha_1}^{\gamma} | S_{m\alpha_2}^{\gamma} \rangle_{\tau}. \quad (3)$$

Here τ represents the imaginary time and T_{τ} represents the imaginary time ordering operator. The notation $S_{n\alpha}^{\gamma}$

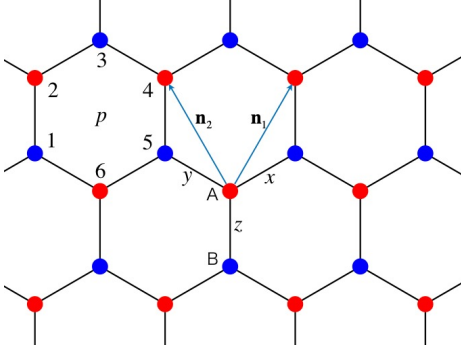


FIG. 1. (Color online) Kitaev model on the honeycomb lattice, showing two interpenetrating sublattices, A and B. Sublattice A is represented by red circles, while sublattice B is represented by blue circles. The direction-dependent interactions in Eq. (1) are labeled as x , y , and z . The lattice vectors are denoted as $\mathbf{n}_1 = (\sqrt{3}/2, 3/2)a_0$ and $\mathbf{n}_2 = (-\sqrt{3}/2, 3/2)a_0$, where a_0 is the nearest neighbor distance. The plaquette operator W_p for plaquette p is defined by Eq. (2).

represents the γ -th component of the spin operator for the α -th sublattice within the n -th unit cell.

Before delving into the analysis of the Green's function, we first discuss its physical meaning. Specifically, we consider the Green's function (3) with $\gamma = x$, $\alpha_1 = B$, and $\alpha_2 = A$. This Green's function describes a process where the \mathbb{Z}_2 flux values at adjacent hexagon plaquettes are flipped at imaginary time 0 and then flipped again at imaginary time τ . This process is schematically illustrated in Fig. 2. We observe that any flipped \mathbb{Z}_2 flux values must be flipped again; otherwise, the thermal average will vanish.

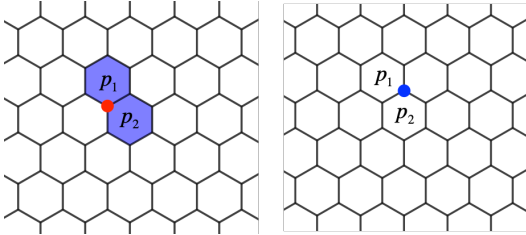


FIG. 2. (Color online) The physical meaning of the Green's function (3) for the case of $\gamma = x$, $\alpha_1 = B$, and $\alpha_2 = A$, with the n -th unit cell shifted from the m -th unit cell by \mathbf{n}_1 . In the left panel, the red circle denotes the A sublattice in the m -th unit cell. At imaginary time 0, the \mathbb{Z}_2 flux values in plaquettes p_1 and p_2 are flipped by the spin operator S_{mA}^x , as indicated by the filled hexagons. In the right panel, the flipped \mathbb{Z}_2 flux values are flipped again at imaginary time τ by the spin operator S_{nB}^x .

Denoting the inverse temperature by $\beta = 1/T$, where T is the temperature, and setting the Boltzmann constant k_B to 1, the Fourier representation of Eq. (3) in the Matsubara frequency, $\omega_n = 2\pi n/\beta$ with n being an

integer, is given by

$$\begin{aligned} G_{n\alpha_1, m\alpha_2}^\gamma(i\omega_n) &= \int_0^\beta d\tau e^{i\omega_n\tau} G_{n\alpha_1, m\alpha_2}^\gamma(\tau) \\ &\equiv \langle S_{n\alpha_1}^\gamma | S_{m\alpha_2}^\gamma \rangle_{i\omega_n} \end{aligned} \quad (4)$$

To find the expression for the Green's function, we first take the derivative of Eq. (3) with respect to τ and then perform the Fourier transform. This process yields

$$\begin{aligned} i\omega_n \langle S_{n\alpha_1}^\gamma | S_{m\alpha_2}^\gamma \rangle_{i\omega_n} &= \langle [\mathcal{H}, S_{n\alpha_1}^\gamma] | S_{m\alpha_2}^\gamma \rangle_{i\omega_n} \\ &+ \langle [S_{n\alpha_1}^\gamma, S_{m\alpha_2}^\gamma] \rangle. \end{aligned} \quad (5)$$

Now we have a new Green's function, represented by the first term on the right-hand side. The equation of motion for this Green's function is given by

$$\begin{aligned} i\omega_n \langle [\mathcal{H}, S_{n\alpha_1}^\gamma] | S_{m\alpha_2}^\gamma \rangle_{i\omega_n} &= \langle [\mathcal{H}, [\mathcal{H}, S_{n\alpha_1}^\gamma]] | S_{m\alpha_2}^\gamma \rangle_{i\omega_n} \\ &+ \langle [[\mathcal{H}, S_{n\alpha_1}^\gamma], S_{m\alpha_2}^\gamma] \rangle. \end{aligned} \quad (6)$$

We first compute $[\mathcal{H}, S_{n\alpha_1}^\gamma]$, and then compute $[\mathcal{H}, [\mathcal{H}, S_{n\alpha_1}^\gamma]]$. From the latter calculation, terms like $\langle S_{nA}^\gamma S_{n_1B}^x S_{n_2A}^\gamma | S_{m\alpha}^x \rangle_{i\omega_n}$, $\langle S_n^\gamma S_{n_1B}^\gamma S_{n_2A}^x | S_{m\alpha}^x \rangle_{i\omega_n}$, etc., appear. Instead of considering the equation of motion for such terms, we approximate them as the product of a correlation function and a Green's function with a reduced number of spins, using the so-called Tyablikov decoupling¹⁰, as follows:

$$\begin{aligned} \langle S_{nA}^\gamma S_{n_1B}^x S_{n_2A}^\gamma | S_{m\alpha}^x \rangle_{i\omega_n} &\simeq \alpha c_{AA}^\gamma (\mathbf{R}_{n_2} - \mathbf{R}_n) \\ &\times \langle S_{n_1B}^x | S_{m\alpha}^x \rangle_{i\omega_n}, \end{aligned} \quad (7)$$

$$\begin{aligned} \langle S_{nA}^\gamma S_{n_1B}^\gamma S_{n_2A}^x | S_{m\alpha}^x \rangle_{i\omega_n} &\simeq \alpha c_{AB}^\gamma (\mathbf{R}_{n_1} - \mathbf{R}_n) \\ &\times \langle S_{n_2A}^x | S_{m\alpha}^x \rangle_{i\omega_n}, \end{aligned} \quad (8)$$

where α is a correction parameter in this approximation⁷ to be determined from the constraint. The approximation is more accurate when one applies this decoupling scheme at Green's functions with more spins or in higher spatial dimensions¹¹. Here, the correlation functions are defined by

$$c_{\alpha_1\alpha_2}^\gamma(\mathbf{R}_{n_2} - \mathbf{R}_{n_1}) = \langle S_{n_1\alpha_1}^\gamma S_{n_2\alpha_2}^\gamma \rangle \quad (9)$$

with \mathbf{R}_n being the coordinate vector of the n -th unit cell.

After a tedious but straightforward calculation followed by a Fourier transform to momentum space, we obtain

$$\left[(i\omega_n)^2 - \frac{K^2}{2} \right] G^x(\mathbf{q}, i\omega_n) - K^2 M(\mathbf{q}) G^x(\mathbf{q}, i\omega_n) \simeq KN(\mathbf{q}). \quad (10)$$

The matrix form of the Green's function, $G^x(\mathbf{q}, i\omega_n)$, is given by:

$$G^x(\mathbf{q}, i\omega_n) = \begin{pmatrix} G_{AA}^x(\mathbf{q}, i\omega_n) & G_{AB}^x(\mathbf{q}, i\omega_n) \\ G_{BA}^x(\mathbf{q}, i\omega_n) & G_{BB}^x(\mathbf{q}, i\omega_n) \end{pmatrix}. \quad (11)$$

The components of the matrices $M(\mathbf{q})$ and $N(\mathbf{q})$ are:

$$M_{AA}(\mathbf{q})/\alpha = c_{AB}^y(0) e^{i\mathbf{q}\cdot\mathbf{n}_1} + c_{AB}^z(\mathbf{n}_2) e^{i\mathbf{q}\cdot(\mathbf{n}_1-\mathbf{n}_2)}, \quad (12)$$

$$M_{AB}(\mathbf{q})/\alpha = -c_{AA}^y(-\mathbf{n}_2) - [c_{AB}^z(0) + c_{AB}^y(\mathbf{n}_2)] e^{-i\mathbf{q}\cdot\mathbf{n}_1} - c_{AA}^z(\mathbf{n}_2) e^{-i\mathbf{q}\cdot\mathbf{n}_2}, \quad (13)$$

$$M_{BA}(\mathbf{q})/\alpha = -c_{BB}^y(\mathbf{n}_2) - [c_{BA}^z(0) + c_{BA}^y(-\mathbf{n}_2)] e^{i\mathbf{q}\cdot\mathbf{n}_1} - c_{BB}^z(-\mathbf{n}_2) e^{i\mathbf{q}\cdot\mathbf{n}_2}, \quad (14)$$

$$M_{BB}(\mathbf{q})/\alpha = c_{BA}^y(0) e^{-i\mathbf{q}\cdot\mathbf{n}_1} + c_{BA}^z(-\mathbf{n}_2) e^{-i\mathbf{q}\cdot(\mathbf{n}_1-\mathbf{n}_2)}. \quad (15)$$

and

$$\begin{aligned} N_{AA}(\mathbf{q}) &= c_{AB}^z(0) + c_{AB}^y(\mathbf{n}_2) \\ N_{AB}(\mathbf{q}) &= -c_{AB}^y(0) - c_{AB}^z(\mathbf{n}_2) e^{-i\mathbf{n}_2\cdot\mathbf{q}} \\ N_{BA}(\mathbf{q}) &= -c_{BA}^y(0) - c_{BA}^z(-\mathbf{n}_2) e^{i\mathbf{n}_2\cdot\mathbf{q}} \\ N_{BB}(\mathbf{q}) &= c_{BA}^z(0) + c_{BA}^y(-\mathbf{n}_2), \end{aligned} \quad (16)$$

respectively. We obtain a similar formula for $G^y(\mathbf{q}, i\omega_n)$ and $G^z(\mathbf{q}, i\omega_n)$. However, due to the symmetry of the honeycomb lattice, we do not need these for the isotropic case.

Solving Eq. (10), we obtain

$$G^x(\mathbf{q}, i\omega_n) = \frac{K}{\left[(i\omega_n)^2 - (\omega_{\mathbf{q}}^{(+)})^2 \right] \left[(i\omega_n)^2 - (\omega_{\mathbf{q}}^{(-)})^2 \right]} \times \begin{pmatrix} (i\omega_n)^2 - K^2/2 - a_{\mathbf{q}}^* & b_{\mathbf{q}} \\ b_{\mathbf{q}}^* & (i\omega_n)^2 - K^2/2 - a_{\mathbf{q}} \end{pmatrix} N_{\mathbf{q}}, \quad (17)$$

The energy dispersion $\omega_{\mathbf{q}}^{(\pm)}$ is given by

$$\omega_{\mathbf{q}}^{(\pm)} = \sqrt{\frac{K^2}{2} + \text{Re}a_{\mathbf{q}} \pm \lambda_{\mathbf{q}}}, \quad (18)$$

with $\lambda_{\mathbf{q}} = \sqrt{|b_{\mathbf{q}}|^2 - |\text{Im}a_{\mathbf{q}}|^2}$. The terms $a_{\mathbf{q}}$ and $b_{\mathbf{q}}$ are defined by

$$a_{\mathbf{q}} = +\alpha K^2 e^{i\mathbf{q}\cdot\mathbf{n}_1} [c_{AB}^y(0) + c_{AB}^z(\mathbf{n}_2) e^{-i\mathbf{q}\cdot\mathbf{n}_2}], \quad (19)$$

$$b_{\mathbf{q}} = -\alpha K^2 [c_{AB}^z(0) e^{-i\mathbf{q}\cdot\mathbf{n}_1} + c_{AB}^y(\mathbf{n}_2) e^{-i\mathbf{q}\cdot\mathbf{n}_1} + c_{AA}^y(-\mathbf{n}_2) + c_{AA}^z(\mathbf{n}_2) e^{-i\mathbf{q}\cdot\mathbf{n}_2}], \quad (20)$$

In our Green's function approach, we determine the correlation functions in a self-consistent manner. The correlation functions are expressed in terms of the Green's function as

$$c_{\alpha_1\alpha_2}^x(\mathbf{r}) = -\frac{1}{N} \sum_{\mathbf{q}} e^{i\mathbf{q}\cdot\mathbf{r}} [G^x(\mathbf{q}, \tau = 0^+)]_{\alpha_1\alpha_2}, \quad (21)$$

where N is the number of unit cells. In the numerical calculations below, we take $N = 45 \times 45$. There are relationships between the correlation functions due to the

absence of magnetic long-range order and any symmetry breaking. By utilizing these symmetries, we define

$$c_1 \equiv c_{AB}^z(0) = c_{AB}^x(\mathbf{n}_1) = c_{AB}^y(\mathbf{n}_2), \quad (22)$$

$$\begin{aligned} c'_1 &\equiv c_{AB}^x(0) = c_{AB}^y(\mathbf{n}_1) = c_{AB}^z(\mathbf{n}_2) \\ &= c_{AB}^y(0) = c_{AB}^z(\mathbf{n}_1) = c_{AB}^x(\mathbf{n}_2), \end{aligned} \quad (23)$$

$$\begin{aligned} c_2 &\equiv c_{AA}^y(\mathbf{n}_2) = c_{AA}^x(\mathbf{n}_1 - \mathbf{n}_2) = c_{AA}^z(\mathbf{n}_1) \\ &= c_{AA}^z(\mathbf{n}_2) = c_{AA}^y(\mathbf{n}_1 - \mathbf{n}_2) = c_{AA}^x(\mathbf{n}_1). \end{aligned} \quad (24)$$

The self-consistent equations to be solved are then given by

$$c_1 = \frac{1}{\beta N} \sum_{\mathbf{q}} \sum_{s=\pm} e^{i\mathbf{q}\cdot\mathbf{n}_1} \frac{Z_{AB}^s}{(\omega_{\mathbf{q}}^s)^2} g\left(\frac{\beta\omega_{\mathbf{q}}^s}{2}\right) \quad (25)$$

$$c'_1 = \frac{1}{\beta N} \sum_{\mathbf{q}} \sum_{s=\pm} \frac{Z_{AB}^s}{(\omega_{\mathbf{q}}^s)^2} g\left(\frac{\beta\omega_{\mathbf{q}}^s}{2}\right) \quad (26)$$

$$c_2 = \frac{1}{\beta N} \sum_{\mathbf{q}} \sum_{s=\pm} e^{i\mathbf{q}\cdot(\mathbf{n}_1-\mathbf{n}_2)} \frac{Z_{AA}^s}{(\omega_{\mathbf{q}}^s)^2} g\left(\frac{\beta\omega_{\mathbf{q}}^s}{2}\right) \quad (27)$$

$$\frac{1}{4} = \frac{1}{\beta N} \sum_{\mathbf{q}} \sum_{s=\pm} \frac{Z_{AA}^s}{(\omega_{\mathbf{q}}^s)^2} g\left(\frac{\beta\omega_{\mathbf{q}}^s}{2}\right) \quad (28)$$

where $g(x) = x \coth x$. The last equation is obtained from $c_{AA}^x(0) = 1/4$. Z_{AA}^{\pm} and Z_{AB}^{\pm} are given by

$$Z_{AA}^{\pm} = \pm \frac{2(i\text{Im}a_{\mathbf{q}} \pm \lambda_{\mathbf{q}}) c_1 + b_{\mathbf{q}} (e^{i\mathbf{n}_2\cdot\mathbf{q}} + 1) c'_1}{2\lambda_{\mathbf{q}}}, \quad (29)$$

$$Z_{AB}^{\pm} = \mp \frac{(e^{-i\mathbf{n}_2\cdot\mathbf{q}} + 1) (i\text{Im}a_{\mathbf{q}} \pm \lambda_{\mathbf{q}}) c'_1 + 2b_{\mathbf{q}} c_1}{2\lambda_{\mathbf{q}}}. \quad (30)$$

The temperature dependencies of c_1 , c'_1 , and c_2 are shown in the left panel of Fig. 3. The value of $4c_1$ converges to 0.4859 as T approaches zero, closely approximating the exact value⁸ of $0.5249 \equiv 4c_1^{\text{exact}}$. At high temperatures, the behavior of c_1 aligns well with the high-temperature expansion result, expressed as $c_1 = \beta K/16 + O(\beta^3)$. Meanwhile, c'_1 and c_2 remain zero across all temperatures, a finding rigorously confirmed⁸ at $T = 0$ and consistent even at finite temperatures. The vanishing of c'_1 and c_2 can be understood as follows. Consider, for instance, $c_{AB}^x(0) = \langle S_{0A}^x S_{0B}^x \rangle$, which corresponds to c'_1 . In this correlation function, the spin operator S_{0B}^x flips the \mathbb{Z}_2 flux values of the adjacent hexagons that share the x -bond emanating from the B sublattice in the 0-th unit cell. Similarly, the spin operator S_{0A}^x flips the \mathbb{Z}_2 flux values of the adjacent hexagons that share the x -bond emanating from the A sublattice in the 0-th unit cell. Since the hexagons affected by S_{0B}^x and S_{0A}^x are different and the Hamiltonian H does not alter the \mathbb{Z}_2 flux values, the thermal average of their product is identically zero. This reasoning also applies to the other

correlation functions, highlighting a unique characteristic of the Kitaev model. The same argument leads to $\langle T_\tau S_{n\alpha_1}^{\gamma_1}(\tau) S_{m\alpha_2}^{\gamma_2}(0) \rangle \equiv 0$ for $\gamma_1 \neq \gamma_2$. The flux values flipped by $S_{m\alpha_2}^{\gamma_2}$ at imaginary time 0 cannot be flipped again by $S_{n\alpha_1}^{\gamma_1}$ at imaginary time τ . We note that this result is exact. From this observation, we may restrict the two-spin Green's function to the form of Eq. (3). We also note that the vanishing of c'_1 and c_2 results in $\omega_{\mathbf{q}}^\pm$ forming a flat band, given by $K\sqrt{(1 \pm 4\alpha c_1)/2}$.

In the right panel of Fig. 3, we present the temperature dependence of α . As temperature increases, α approaches one, indicating that the decoupling approximation in Eqs. (7) and (8) becomes exact without the need for the correction parameter α . However, deviations of α from one at lower temperatures suggest the necessity of this correction parameter in the equations.

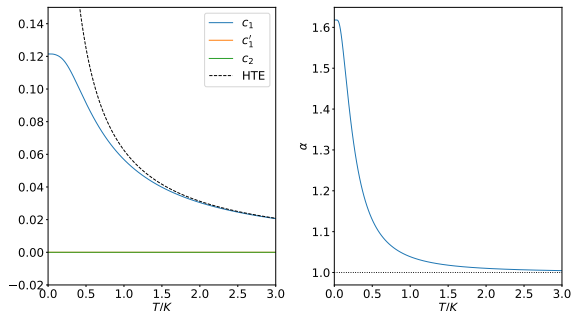


FIG. 3. (Color online) Temperature dependence of the correlation functions and the correction parameter α . Left panel: The temperature dependencies of c_1 , c'_1 , and c_2 are shown. The value of $4c_1$ approaches the exact theoretical value⁸ of 0.5249 at $T = 0$ and aligns with high-temperature expansion result, which is indicated by the dashed line, at elevated temperatures, while c'_1 and c_2 remain zero across the temperature range. Right panel: The variation of the parameter α with temperature, demonstrating the exactness of the decoupling approximation at high temperatures (where α approaches 1) and the necessity of this correction parameter at lower temperatures, where α deviates from 1.

From the temperature dependence of c_1 , the internal energy can be computed using the relation

$$E = \langle H \rangle = -\frac{3}{4}NKc_1. \quad (31)$$

We compared the temperature dependence of the energy with the results shown in Fig. 15(a) of Ref. 12, as shown in Fig. 4(a). We found an almost perfect match for $T > T_H$ with $T_H \simeq 0.375K$, but our energy values are slightly higher for $T < T_H$. This discrepancy likely originates from the error in the c_1 value at $T = 0$. Although the relative error is $|(c_1^{\text{exact}} - c_1)/c_1^{\text{exact}}| \simeq 0.07$, minor details and significant physics, such as the fractionalization of spins, may be hidden within this discrepancy.

Figure 4 shows the temperature dependencies of the specific heat and entropy. The specific heat is calculated from the temperature derivative of the internal energy

E and compared with the high-temperature expansion (HTE) result, $C_{\text{HTE}} = 3NK^2\beta^2/16$. The entropy is computed using the formula:

$$S = S(\infty) - \int_T^{T_0} dT \frac{C(T)}{T} - \int_{T_0}^{\infty} dT \frac{C_{\text{HTE}}(T)}{T}, \quad (32)$$

where $S(\infty) = 2N \ln 2$ and T_0 is a sufficiently large value at which the Green's function result for the specific heat closely approximates the HTE result (here, we take $T_0/K = 10$). The specific heat exhibits a single broad peak around $T/K \simeq 0.4$, consistent with mean field calculations¹³. We likely fail to observe the low-temperature peak around $T_L \simeq 0.012K$ reported in Ref. 14 due to the discrepancy mentioned above. The entropy indicates the presence of residual entropy, but if fractionalization were captured, this residual entropy should vanish, as it has been rigorously shown that there are no \mathbb{Z}_2 fluxes in the ground state and the system must satisfy the third law of thermodynamics.

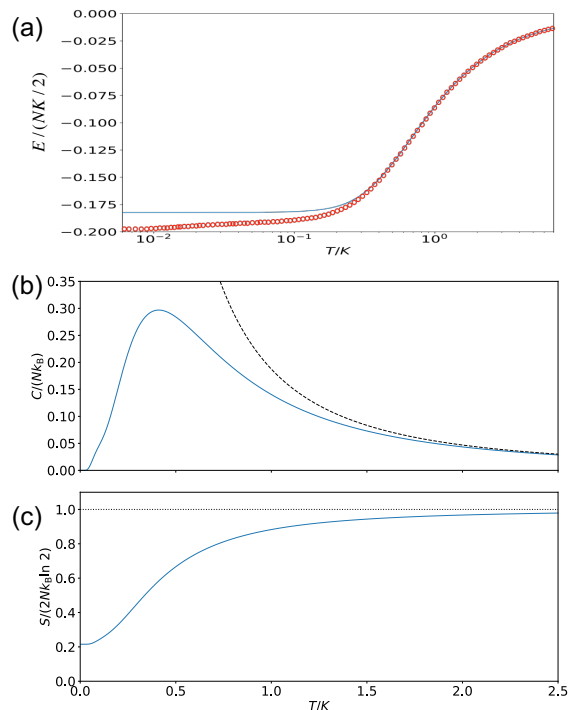


FIG. 4. (Color online) Temperature dependencies of (a) the energy $E = -3NKc_1/4$, (b) specific heat, and (c) entropy. The red circles in (a) are data taken from Ref. 12. The specific heat, calculated from the temperature derivative of the internal energy E , is compared with the high-temperature expansion result $C_{\text{HTE}} = 3NK^2\beta^2/16$. It displays a broad peak around $T/K \simeq 0.4$ without any lower-temperature peaks. The entropy is computed based on Eq. (32).

In conclusion, we have investigated the Kitaev model at finite temperatures using a Green's function approach that maintains $SU(2)$ symmetry. Our computations of the temperature dependence of the correlation functions

revealed that the nearest neighbor spin-spin correlation functions closely match the exact values at zero temperature. Additionally, we have presented several exact results concerning the spin Green's function and spin-spin correlation functions specific to the Kitaev model. These findings enhance our understanding of the Kitaev model and provide a novel approach to this model without relying on Majorana fermions. This work opens up new

avenues for exploring the dynamic properties of the Kitaev model and its applications in the study of quantum spin liquids and topological quantum computing.

ACKNOWLEDGMENTS

The authors thank K. Harada and D. Sasamoto for helpful discussions.

* takegami.hibiki.64h@st.kyoto-u.ac.jp

† morinari.takao.5s@kyoto-u.ac.jp

¹ L. Savary and L. Balents, Rep. Progr. Phys. **80**, 016502 (2017).

² A. Kitaev, Ann. Phys. **321**, 2 (2006).

³ G. Jackeli and G. Khaliullin, Phys. Rev. Lett. **102**, 017205 (2009).

⁴ H. Takagi, T. Takayama, G. Jackeli, G. Khaliullin, and S. E. Nagler, Nat. Rev. Phys. **1**, 264 (2019).

⁵ A. Kitaev, Ann. Phys. **303**, 2 (2003).

⁶ C. Nayak, S. H. Simon, A. Stern, M. Freedman, and S. Das Sarma, Rev. Mod. Phys. **80**, 1083 (2008).

⁷ J. Kondo and K. Yamaji, Progr. Theoret. Phys. **47**, 807 (1972).

⁸ G. Baskaran, S. Mandal, and R. Shankar, Phys. Rev. Lett. **98**, 247201 (2007).

⁹ D. N. Zubarev, Sov. Phys. Usp. **3**, 320 (1960).

¹⁰ S. Tyablikov and V. Bonch-Bruевич, Adv. Phys. **11**, 317 (1962).

¹¹ D. Sasamoto and T. Morinari, J. Phys. Soc. Jpn. **93**, 024704 (2024).

¹² Y. Motome and J. Nasu, J. Phys. Soc. Jpn. **89**, 012002 (2020).

¹³ S. G. Saheli, J. Lin, H. Hu, and F. Krüger, Phys. Rev. B **109**, 014407 (2024).

¹⁴ J. Nasu, M. Udagawa, and Y. Motome, Phys. Rev. B **92**, 115122 (2015).